



1 **Analysis of Groundwater Response to Oscillatory Pumping Test in**
2 **Unconfined Aquifers: Consider the Effects of Initial Condition and**
3 **Wellbore Storage**

4 **Ching-Sheng Huang^a, Ya-Hsin Tsai^b, Hund-Der Yeh^{b*} and Tao Yang^{a*}**

5 ^a State Key Laboratory of Hydrology-Water Resources and Hydraulic Engineering, Center for
6 Global Change and Water Cycle, Hohai University, Nanjing 210098, China

7 ^b Institute of Environmental Engineering, National Chiao Tung University, Hsinchu 300,
8 Taiwan

9 * Corresponding authors:

10 Hund-Der Yeh; E-mail: hdyeh@mail.nctu.edu.tw; Tel.: +886-3-5731910; fax: +886-3-
11 5725958

12 Tao Yang; E-mail: tao.yang@hhu.edu.cn; Tel.: +86-13770918075

13
14 Submission to *Hydrology and Earth System Sciences* on 12 April 2018

15
16 **Key points**

- 17 1. An analytical solution of the hydraulic head due to oscillatory pumping test in unconfined
18 aquifers is presented.
19 2. The effects of wellbore storage and initial condition of static groundwater before the test
20 are analyzed.
21 3. The present solution agrees well to head fluctuation data taken from a field oscillatory
22 pumping test.



Abstract

Oscillatory pumping test (OPT) is an alternative to constant-head and constant-rate pumping tests for determining aquifer hydraulic parameters without water extraction. There is a large number of analytical models presented for the analyses of OPT. The combined effects of wellbore storage and initial condition regarding the hydraulic head prior to OPT are commonly neglected in the existing models. This study aims to develop a new model for describing the hydraulic head fluctuation induced by OPT in an unconfined aquifer. The model contains a typical flow equation with an initial condition of static water table, inner boundary condition specified at the rim of a finite-radius well for incorporating wellbore storage effect, and linearized free surface equation describing water table movement. The analytical solution of the model is derived by the Laplace transform and finite integral transform. Sensitivity analysis is carried out for exploring head response to the change in each of hydraulic parameters. Results suggest that head fluctuation due to OPT starts from the initial condition and gradually tends to simple harmonic motion (SHM) after a certain pumping time. A criterion for estimating the time to have SHM since OPT is graphically presented. The validity of assuming an infinitesimal well radius without wellbore storage effect is investigated. The present solution agrees well to head fluctuation data observed at the Boise hydrogeophysical research site in southwestern Idaho.

KEYWORDS: oscillatory pumping test, analytical solution, free surface equation, initial condition, wellbore storage



43

NOTATION

a	σ/μ
b	Aquifer thickness
\bar{b}	Dimensionless aquifer thickness, i.e., $\bar{b} = b/r_w$
h	Hydraulic head
\bar{h}	Dimensionless Hydraulic head, i.e., $\bar{h} = (2\pi b K_r h)/ Q $
K_r, K_z	Aquifer horizontal and vertical hydraulic conductivities, respectively
P	Period of oscillatory pumping rate
p	Laplace parameter
Q	Amplitude of oscillatory pumping rate
R	Radius of influence
\bar{R}	Dimensionless radius of influence, i.e., $\bar{R} = R/r_w$
r	Radial distance from the center of pumping well
\bar{r}	Dimensionless radial distance, i.e., $\bar{r} = r/r_w$
r_c	Outer radius of pumping well
r_w	Inner radius of pumping well
S_s, S_y	Specific storage and specific yield, respectively
t	Time since pumping
\bar{t}	Dimensionless pumping time, i.e., $\bar{t} = (K_r t)/(S_s r_w^2)$
z	Elevation from aquifer bottom
\bar{z}	Dimensionless elevation, i.e., $\bar{z} = z/b$
α	$r_c^2/(2r_w^2 S_s b)$
β_n, β_m	Roots of Eqs. (19) and (36), respectively
γ	$S_s r_w^2 \omega/K_r$
κ	K_z/K_r
μ	κ/\bar{b}^2
σ	$S_y/(S_s b)$
ω	Frequency of oscillatory pumping rate, i.e., $\omega = 2\pi/P$

44



1. Introduction

Numerous attempts have been made by researchers to the study of oscillatory pumping test (OPT) that is an alternative to constant-rate and constant-head pumping tests for determining aquifer hydraulic parameters (e.g., Vine et al., 2016; Christensen et al., 2017; Watlet et al., 2018). The concept of OPT was first proposed by Kuo (1972) in the petroleum literature. The process of OPT contains extraction stages and injection stages. The pumping rate, in other words, varies periodically as a sinusoidal function of time. Compared with traditional constant-rate pumping, OPT in contaminated aquifers has the following advantages: (1) low cost because of no disposing contaminated water from the well, (2) reduced risk of treating contaminated fluid, (3) smaller contaminant movement, and (4) stable signal easily distinguished from background disturbance such as tide effect and varying river stage (e.g., Spane and Mackley, 2011). However, OPT has the disadvantages including the need of an advanced apparatus producing periodic rate and the problem of signal attenuation in remote distance from the pumping well. Oscillatory hydraulic tomography adopts several oscillatory pumping wells with different frequencies (e.g., Yeh and Liu, 2000; Cardiff et al., 2013; Zhou et al., 2016; Muthuwatta, et al., 2017). Aquifer heterogeneity can be mapped by analyzing multiple data collected from observation wells. Cardiff and Barrash (2011) reviewed articles associated with hydraulic tomography and classified them according to nine categories in a table.

Various groups of researchers have worked with analytical and numerical models for OPT; each group has its own model and investigation. For example, Black and Kipp (1981) assumed the response of confined flow to OPT as simple harmonic motion (SHM) in the absence of an initial condition. Cardiff and Barrash (2014) built an optimization formulation strategy using the Black and Kipp analytical solution. Dagan and Rabinovich (2014) also assumed hydraulic head fluctuation as SHM for OPT at a partially penetrating well in unconfined aquifers. Cardiff et al. (2013) characterized aquifer heterogeneity using the finite element-based COMSOL software that adopts SHM hydraulic head variation for OPT. On the other hand, Rasmussen et



71 al. (2003) found that hydraulic head response tends to SHM after a certain period of pumping
72 time when considering an initial condition prior to OPT. Bakhos et al. (2014) used the
73 Rasmussen et al. (2003) analytical solution to quantify the time after which hydraulic head
74 fluctuation can be regarded as SHM since OPT began. As shown above, existing models for
75 OPT have either assumed hydraulic head fluctuation as SHM without an initial condition or
76 ignored the effect of wellbore storage with considering an infinitesimal well radius.

77 Field applications of OPT for determining aquifer parameters have been conducted in
78 recent years. Rasmussen et al. (2003) estimated aquifer hydraulic parameters based on 1 – 2.5-
79 hour period of OPT at the Savannah River site. Mainault et al. (2008) observed spontaneous
80 potential temporal variation in aquifer diffusivity at a study site in Bochum, Germany. Fokker
81 et al. (2012; 2013) presented spatial distributions of aquifer transmission and storage
82 coefficient derived from curve fitting based on a numerical model and field data from
83 experiments at the southern city-limits of Bochum, Germany. Rabinovich et al. (2015)
84 estimated aquifer parameters of equivalent hydraulic conductivity, specific storage and specific
85 yield at the Boise Hydrogeophysical Research Site (BHRS) by curve fitting based on
86 observation data and the Dagan and Rabinovich analytical solution. They conclude that the
87 equivalent hydraulic parameters can represent the actual aquifer heterogeneity of the study site.

88 Although a large number of studies have been made on development of analytical models
89 for OPT, little is known about the combined effects of wellbore storage and initial condition
90 prior to OPT. Analytical solution to such a question will not only have important physical
91 implications but also shed light on OPT model development. This study builds an improved
92 model describing hydraulic head fluctuation induced by OPT in an unconfined aquifer. The
93 model is composed of a typical flow equation with the initial condition of static water table, an
94 inner boundary condition specified at the rim of the pumping well for incorporating wellbore
95 storage effect, and a first-order free surface equation describing the movement of aquifer water
96 table. The analytical solution of the model is derived by the methods of Laplace transform and
97 finite integral transform. Based on the present solution, sensitivity analysis is performed to



198 explore the hydraulic head in response to the change in each of hydraulic parameters. The
199 quantitative criteria for excluding the individual effects of wellbore storage and the initial
200 condition are discussed. The radius of influence induced by OPT is investigated for engineering
201 applications. In addition, curve fitting of the present solution to head fluctuation data recorded
202 at BHRS is presented.

203 **2. Methodology**

204 **2.1. Mathematical model**

205 Consider an oscillatory pumping at a fully penetrating well in an unconfined aquifer illustrated
206 in Fig. 1. The aquifer is of unbound lateral extent with a finite thickness b . The radial distance
207 from the centerline of the well is r ; an elevation from the impermeable bottom of the aquifer is
208 z . The well has inner radius r_c and outer radius r_w .

209 The flow equation describing spatiotemporal head distribution in aquifers can be written
210 as:

$$211 \quad K_r \left(\frac{\partial^2 h}{\partial r^2} + \frac{1}{r} \frac{\partial h}{\partial r} \right) + K_z \frac{\partial^2 h}{\partial z^2} = S_s \frac{\partial h}{\partial t} \quad \text{for } r_w \leq r < \infty, 0 \leq z \leq b \text{ and } t \geq 0 \quad (1)$$

212 where $h(r, z, t)$ is hydraulic head at location (r, z) and time t ; K_r and K_z are respectively
213 the radial and vertical hydraulic conductivities; S_s is the specific storage. Consider water table
214 as a reference datum where the elevation head is set to zero; the initial condition is expressed
215 as:

$$216 \quad h = 0 \text{ at } t = 0 \quad (2)$$

217 The rim of the wellbore is regarded as an inner boundary, which provides the associated
218 condition as:

$$219 \quad 2\pi r_w K_r b \frac{\partial h}{\partial r} = Q \sin(\omega t) + \pi r_c^2 \frac{\partial h}{\partial t} \text{ at } r=r_w \quad (3)$$

220 where Q and ω are respectively the amplitude and frequency of oscillatory pumping rate; is
221 frequency. The first term on the right-hand side (RHS) of Eq. (3) represents an oscillatory
222 pumping rate, and the second term represents the volume change within the well reflecting
223 wellbore storage effect. Water table movement can be defined by the first-order free surface



equation proposed by Neuman (1972) as

$$K_z \frac{\partial h}{\partial z} = -S_y \frac{\partial h}{\partial t} \quad \text{at } z = b \quad (4)$$

where S_y is the specific yield. The impervious aquifer bottom is under the no-flow condition:

$$\frac{\partial h}{\partial z} = 0 \quad \text{at } z = 0 \quad (5)$$

The hydraulic head far away from the well remains constant and is expressed as

$$\lim_{r \rightarrow \infty} h(r, z, t) = 0 \quad (6)$$

Define dimensionless variables and parameters as follows:

$$\begin{aligned} \bar{h} &= \frac{2\pi b K_r}{Q} h, \quad \bar{r} = \frac{r}{r_w}, \quad \bar{z} = \frac{z}{b}, \quad \bar{t} = \frac{K_r}{S_s r_w^2} t, \quad \bar{b} = \frac{b}{r_w}, \\ \alpha &= \frac{r_c^2}{2 r_w^2 S_s b}, \quad \gamma = \frac{S_s r_w^2}{K_r} \omega, \quad \kappa = \frac{K_z}{K_r}, \quad \mu = \frac{\kappa}{\bar{b}^2}, \quad \sigma = \frac{S_y}{S_s b}, \quad a = \frac{\sigma}{\mu} \end{aligned} \quad (7)$$

where the overbar stands for a dimensionless symbol. Note that the magnitude of α dominates wellbore storage effect (Papadopoulos and Cooper, 1967) and γ is a dimensionless frequency parameter. With Eq. (7), the dimensionless forms of Eqs. (1) - (6) become, respectively,

$$\frac{\partial^2 \bar{h}}{\partial \bar{r}^2} + \frac{1}{\bar{r}} \frac{\partial \bar{h}}{\partial \bar{r}} + \mu \frac{\partial^2 \bar{h}}{\partial \bar{z}^2} = \frac{\partial \bar{h}}{\partial \bar{t}} \quad \text{for } 1 \leq \bar{r} < \infty, \quad 0 \leq \bar{z} < 1 \quad \text{and } \bar{t} \geq 0 \quad (8)$$

$$\bar{h} = 0 \quad \text{at } \bar{t} = 0 \quad (9)$$

$$\frac{\partial \bar{h}}{\partial \bar{r}} = \sin(\gamma \bar{t}) + \alpha \frac{\partial \bar{h}}{\partial \bar{t}} \quad \text{at } \bar{r} = 1 \quad (10)$$

$$\frac{\partial \bar{h}}{\partial \bar{z}} = -a \frac{\partial \bar{h}}{\partial \bar{t}} \quad \text{at } \bar{z} = 1 \quad (11)$$

$$\frac{\partial \bar{h}}{\partial \bar{z}} = 0 \quad \text{at } \bar{z} = 0 \quad (12)$$

$$\lim_{\bar{r} \rightarrow \infty} \bar{h}(\bar{r}, \bar{z}, \bar{t}) = 0 \quad (13)$$

The transient solution of the dimensionless head \bar{h} satisfies Eqs. (8) - (13) with the initial condition Eq. (9). Here we define a pseudo-steady state solution \bar{h}_s to the model of Eqs. (8) and (10) - (13) with $\sin(\gamma \bar{t})$ in Eq. (10) replaced by $\text{Im}(e^{i\gamma \bar{t}})$, $\text{Im}(-)$ being the imaginary part of a complex number, and i being the imaginary unit. The pseudo-steady state model accounts for SHM of head fluctuation after a certain period of pumping time.



2.2. Transient solution for unconfined aquifer

The Laplace transform and finite integral transform are applied to solve Eqs. (8) - (13) (Liang et al., 2017). The former converts $\bar{h}(\bar{r}, \bar{z}, \bar{t})$ into $\hat{h}(\bar{r}, \bar{z}, p)$, $\partial \bar{h} / \partial \bar{t}$ in Eq. (8), (10) and (11) into $p \hat{h}$, and $\sin(\gamma \bar{t})$ in Eq. (10) into $\gamma / (p^2 + \gamma^2)$ with the Laplace parameter p . The result of Eq. (8) in the Laplace domain can be written as

$$\frac{\partial^2 \hat{h}}{\partial \bar{r}^2} + \frac{1}{\bar{r}} \frac{\partial \hat{h}}{\partial \bar{r}} + \mu \frac{\partial^2 \hat{h}}{\partial \bar{z}^2} = p \hat{h} \quad (14)$$

The transformed boundary conditions in r and z directions are expressed as

$$\frac{\partial \hat{h}}{\partial \bar{r}} = \frac{\gamma}{p^2 + \gamma^2} + \alpha p \hat{h} \text{ at } \bar{r} = 1 \quad (15)$$

$$\frac{\partial \hat{h}}{\partial \bar{z}} = -\alpha p \hat{h} \text{ at } \bar{z} = 1 \quad (16)$$

$$\frac{\partial \hat{h}}{\partial \bar{z}} = 0 \text{ at } \bar{z} = 0 \quad (17)$$

$$\lim_{\bar{r} \rightarrow \infty} \hat{h}(\bar{r}, \bar{z}, p) = 0 \quad (18)$$

The finite integral transform proposed by Latinopoulos (1985) is applied to Eqs. (14) - (17). The definition of the transform is given in Appendix A. Using the property of the transform converts $\hat{h}(\bar{r}, \bar{z}, p)$ into $\tilde{h}(\bar{r}, \beta_n, p)$, $\mu \partial^2 \hat{h} / \partial \bar{z}^2$ in Eq. (14) into $-\mu \beta_n^2 \tilde{h}$, and $\gamma / (p^2 + \gamma^2)$ in Eq. (15) into $\gamma F_t \sin \beta_n / (p^2 + \gamma^2)$ where $n \in (1, 2, 3, \dots, \infty)$; $F_t = \sqrt{2(\beta_n^2 + a^2 p^2) / (\beta_n^2 + a^2 p^2 + \alpha p)}$; β_n is the positive roots of the equation:

$$\tan \beta_n = \alpha p / \beta_n \quad (19)$$

The method to find the roots of β_n is discussed in section 2.3. Eq. (14) then becomes an ordinary differential equation (ODE) denoted as

$$\frac{\partial^2 \tilde{h}}{\partial \bar{r}^2} + \frac{1}{\bar{r}} \frac{\partial \tilde{h}}{\partial \bar{r}} - \mu \beta_n^2 \tilde{h} = p \tilde{h} \quad (20)$$

with the transformed Eqs. (18) and (15) written, respectively, as

$$\lim_{\bar{r} \rightarrow \infty} \tilde{h}(\bar{r}, \beta_n, p) = 0 \quad (21a)$$

$$\frac{\partial \tilde{h}}{\partial \bar{r}} = \frac{\gamma F_t \sin \beta_n}{\beta_n (p^2 + \gamma^2)} + \alpha p \tilde{h} \text{ at } \bar{r} = 1 \quad (21b)$$

Note that the transformation from Eq. (14) to (20) is applicable only for the no-flow condition



171 specified at $\bar{z} = 0$ (i.e., Eq. (17)) and third-type condition specified at $\bar{z} = 1$ (i.e., Eq. (16)).

172 Solve Eq. (20) with (21a) and (21b), and we obtain:

$$173 \quad \tilde{h}(\bar{r}, \beta_n, p) = -\frac{\gamma F_t \sin \beta_n K_0(r\lambda)}{\beta_n(p^2 + \gamma^2)(p\alpha K_0(\lambda) + \lambda K_1(\lambda))} \quad (22)$$

174 with

$$175 \quad \lambda = \sqrt{p + \mu \beta_n^2} \quad (23)$$

176 where $K_0(-)$ and $K_1(-)$ is the modified Bessel function of the second kind of order zero

177 and one, respectively. Applying the inverse Laplace transform and inverse finite integral

178 transform to Eq. (22) results in the transient solution expressed as

$$179 \quad \bar{h}(\bar{r}, \bar{z}, \bar{t}) = \bar{h}_{\text{exp}}(\bar{r}, \bar{z}, \bar{t}) + \bar{h}_{\text{SHM}}(\bar{r}, \bar{z}, \bar{t}) \quad (24a)$$

180 with

$$181 \quad \bar{h}_{\text{exp}}(\bar{r}, \bar{z}, \bar{t}) = \frac{-2}{\pi} \sum_{n=1}^{\infty} \int_0^{\infty} \cos(\beta_n \bar{z}) \text{Im}(\gamma \varepsilon_1 \varepsilon_2 \exp(p_0 \bar{t})) d\zeta \quad (24b)$$

$$182 \quad \bar{h}_{\text{SHM}}(\bar{r}, \bar{z}, \bar{t}) = \bar{A}_t(\bar{r}, \bar{z}) \cos(\gamma \bar{t} - \phi_t(\bar{r}, \bar{z})) \quad (24c)$$

$$183 \quad \bar{A}_t(\bar{r}, \bar{z}) = \sqrt{a_t(\bar{r}, \bar{z})^2 + b_t(\bar{r}, \bar{z})^2} \quad (24d)$$

$$184 \quad a_t(\bar{r}, \bar{z}) = \frac{2}{\pi} \sum_{n=1}^{\infty} \int_0^{\infty} \cos(\beta_n \bar{z}) \text{Im}(\varepsilon_1 \varepsilon_2 p_0) d\zeta \quad (24e)$$

$$185 \quad b_t(\bar{r}, \bar{z}) = \frac{2\gamma}{\pi} \sum_{n=1}^{\infty} \int_0^{\infty} \cos(\beta_n \bar{z}) \text{Im}(\varepsilon_1 \varepsilon_2) d\zeta \quad (24f)$$

$$186 \quad \phi_t(\bar{r}, \bar{z}) = \cos^{-1}(b_t(\bar{r}, \bar{z})/\bar{A}_t(\bar{r}, \bar{z})) \quad (24g)$$

$$187 \quad \varepsilon_1 = \sin \beta_n K_0(\bar{r}\lambda_0) / (\beta_n(p_0^2 + \gamma^2)(p_0\alpha K_0(\lambda_0) + \lambda_0 K_1(\lambda_0))) \quad (24h)$$

$$188 \quad \varepsilon_2 = (\beta_n^2 + a^2 p_0^2) / (\beta_n^2 + a^2 p_0^2 + a p_0) \quad (24i)$$

$$189 \quad p_0 = -\zeta - \mu \beta_n^2 \quad (24j)$$

$$190 \quad \lambda_0 = \sqrt{\zeta} i \quad (24k)$$

191 The detailed derivation of Eqs. (24a) – (24k) is presented in Appendix B. The first RHS term

192 in Eq. (24a) due to the initial condition exhibits exponential decay since pumping began; the

193 second term defines SHM with amplitude $\bar{A}_t(\bar{r}, \bar{z})$ and phase shift $\phi_t(\bar{r}, \bar{z})$ at a given point

194 (\bar{r}, \bar{z}) . The numerical results of the integrals in Eqs. (24b), (24e) and (24f) are obtained by the

195 Mathematica NIntegrate function.



196 2.3. Calculation of β_n

197 The eigenvalues β_1, \dots, β_n , the roots of Eq. (19) with p replaced by p_0 in Eq. (24j), can
 198 be determined by applying the Mathematica function FindRoot based on Newton's method
 199 with reasonable initial guesses. The roots are located at the intersection of the curves plotted
 200 by the RHS and left-hand side (LHS) functions of β_n in Eq. (19). The roots are very close to
 201 the vertical asymptotes of the periodical tangent function $\tan \beta_n$. The initial guess for each β_n
 202 can be considered as $(2n - 1)\pi/2 + \delta$ where $n \in (1, 2, \dots, \infty)$ and δ is a small positive
 203 value set to 10^{-10} to prevent the denominator in Eq. (19) from zero.

204 2.4. Transient solution for confined aquifer

205 When $S_y = 0$ (i.e., $\sigma = 0$), Eq. (11) reduces to $\partial \bar{h} / \partial \bar{z} = 0$ for a no-flow condition at the top
 206 of the aquifer, indicating that the unconfined aquifer becomes a confined one. Under this
 207 condition, Eq. (19) becomes $\tan \beta_n = 0$ with roots $\beta_n = 0, \pi, 2\pi, \dots, n\pi, \dots, \infty$; Eq. (24i)
 208 reduces to $\varepsilon_2 = 1$; factor 2 in Eqs. (24b), (24e) and (24f) is replaced by unity. The analytical
 209 solution of the transient head for the confined aquifer can be expressed as

$$210 \quad \bar{h}(\bar{r}, \bar{t}) = \bar{h}_{\text{exp}}(\bar{r}, \bar{t}) + \bar{h}_{\text{SHM}}(\bar{r}, \bar{t}) \quad (25a)$$

211 with

$$212 \quad \bar{h}_{\text{exp}}(\bar{r}, \bar{t}) = \frac{-1}{\pi} \int_0^\infty \text{Im}(\varepsilon_1 \gamma \exp(-\zeta \bar{t})) d\zeta \quad (25b)$$

$$213 \quad \bar{h}_{\text{SHM}}(\bar{r}, \bar{t}) = \bar{A}_t(\bar{r}) \cos(\gamma \bar{t} - \phi_t(\bar{r})) \quad (25c)$$

$$214 \quad \bar{A}_t(\bar{r}) = \sqrt{a_t(\bar{r})^2 + b_t(\bar{r})^2} \quad (25d)$$

$$215 \quad a_t(\bar{r}) = \frac{1}{\pi} \int_0^\infty \text{Im}(-\varepsilon_1 \zeta) d\zeta \quad (25e)$$

$$216 \quad b_t(\bar{r}) = \frac{\gamma}{\pi} \int_0^\infty \text{Im}(\varepsilon_1) d\zeta \quad (25f)$$

$$217 \quad \phi_t(\bar{r}) = \cos^{-1}(b_t(\bar{r})/\bar{A}_t(\bar{r})) \quad (25g)$$

$$218 \quad \varepsilon_1 = K_0(\bar{r}\lambda_0)/((p_0^2 + \gamma^2)(-\alpha\zeta K_0(\lambda_0) + \lambda_0 K_1(\lambda_0))) \quad (25h)$$

219 Note that Eq. (24h) reduces to Eq. (25h) based on $\beta_n = 0$ and L' Hospital's rule and gives
 220 $\varepsilon_1 = 0$ for the other roots $\beta_n = \pi, 2\pi, \dots, n\pi$. This causes that Eqs. (25a) – (25h) are
 221 independent of dimensionless elevation \bar{z} , indicating only horizontal flow in the confined



222 aquifer.

223 2.5. Pseudo-steady state solution for unconfined aquifer

224 The pseudo-steady state solution \bar{h}_s satisfies the following form (Dagan and Rabinovich,
 225 2014).

$$226 \quad \bar{h}_s(\bar{r}, \bar{z}, \bar{t}) = \text{Im}(\bar{H}(\bar{r}, \bar{z}) e^{i\gamma\bar{t}}) \quad (26)$$

227 where $\bar{H}(\bar{r}, \bar{z})$ is a space function of \bar{r} and \bar{z} . Substituting Eq. (26) and $\partial\bar{h}_s/\partial\bar{t} =$

228 $\text{Im}(i\gamma\bar{H}(\bar{r}, \bar{z}) e^{i\gamma\bar{t}})$ into the pseudo-steady state model results in

$$229 \quad \frac{\partial^2 \bar{H}}{\partial \bar{r}^2} + \frac{1}{\bar{r}} \frac{\partial \bar{H}}{\partial \bar{r}} + \mu \frac{\partial^2 \bar{H}}{\partial \bar{z}^2} = i\gamma \bar{H} \quad (27)$$

$$230 \quad \frac{\partial \bar{H}}{\partial \bar{r}} = 1 + i\alpha\gamma \bar{H} \text{ at } \bar{r} = 1 \quad (28)$$

$$231 \quad \frac{\partial \bar{H}}{\partial \bar{z}} = -i\alpha\gamma \bar{H} \text{ at } \bar{z} = 1 \quad (29)$$

$$232 \quad \frac{\partial \bar{H}}{\partial \bar{z}} = 0 \text{ at } \bar{z} = 0 \quad (30)$$

$$233 \quad \lim_{\bar{r} \rightarrow \infty} \bar{H} = 0 \quad (31)$$

234 Again, taking the finite integral transform to Eqs. (27) - (31) yields

$$235 \quad \frac{\partial^2 \tilde{H}}{\partial \bar{r}^2} + \frac{1}{\bar{r}} \frac{\partial \tilde{H}}{\partial \bar{r}} - \mu\beta_m^2 \tilde{H} = i\gamma \tilde{H} \quad (32)$$

$$236 \quad \frac{\partial \tilde{H}}{\partial \bar{r}} = \frac{\sin\beta_m}{\beta_m} F_s + i\alpha\gamma \tilde{H} \text{ at } \bar{r} = 1 \quad (33)$$

$$237 \quad \lim_{\bar{r} \rightarrow \infty} \tilde{H} = 0 \quad (34)$$

$$238 \quad F_s = \sqrt{2(\beta_m^2 - a^2\gamma^2)/(\beta_m^2 - a^2\gamma^2 + i\alpha\gamma)} \quad (35)$$

239 where $\beta_m = c_m + d_m i$ is a complex number being the roots of the equation:

$$240 \quad \beta_m \tan \beta_m = i\alpha\gamma \quad (36)$$

241 The method to determine β_m is given in section 2.6. Solving Eq. (32) with (33) and (34)

242 results in

$$243 \quad \tilde{H}(\bar{r}, \beta_m) = F_s \frac{i \sin(\beta_m) K_0(\bar{r}\lambda)}{\beta_m (\alpha\gamma K_0(\lambda) - i\lambda K_1(\lambda))} \quad (37)$$

244 where $\lambda = \sqrt{\gamma i + \mu\beta_m^2}$. After taking the inverse finite integral transform to Eq. (37) and



245 applying the formula of $e^{i\gamma\bar{t}} = \cos(\gamma\bar{t}) + i \sin(\gamma\bar{t})$ to the result, the pseudo-steady state
 246 solution can be expressed as

$$247 \quad \bar{h}_s(\bar{r}, \bar{z}, \bar{t}) = \bar{A}_s(\bar{r}, \bar{z}) \cos(\gamma\bar{t} - \phi_s(\bar{r}, \bar{z})) \quad (38a)$$

248 with

$$249 \quad \bar{A}_s(\bar{r}, \bar{z}) = \sqrt{a_s(\bar{r}, \bar{z})^2 + b_s(\bar{r}, \bar{z})^2} \quad (38b)$$

$$250 \quad a_s(\bar{r}, \bar{z}) = \text{Re}(\sum_{m=1}^{\infty} D(\bar{r}, \beta_m) \cos(\beta_m \bar{z})) \quad (38c)$$

$$251 \quad b_s(\bar{r}, \bar{z}) = \text{Im}(\sum_{m=1}^{\infty} D(\bar{r}, \beta_m) \cos(\beta_m \bar{z})) \quad (38d)$$

$$252 \quad \phi_s(\bar{r}, \bar{z}) = \cos^{-1}(b_s(\bar{r}, \bar{z})/A_s(\bar{r}, \bar{z})) \quad (38e)$$

$$253 \quad D(\bar{r}, \beta_m) = iF_s^2 \sin \beta_m K_0(\bar{r}\lambda) / (\beta_m (\alpha\gamma K_0(\lambda) - i\lambda K_1(\lambda))) \quad (38f)$$

254 where $\text{Re}(-)$ is the real part of a complex number. Eq. (38a) indicates SHM for the response of
 255 the hydraulic head at any point to oscillatory pumping.

256 **2.6 Calculation of β_m**

257 Substituting $\beta_m = c_m + d_m i$ and $\tan \beta_m = \sin(2c_m)/\tau + i \sinh(2d_m)/\tau$ with $\tau =$
 258 $\cos(2c_m) + \cosh(2d_m)$ into Eq. (36) and separating the real and imaginary parts of the result
 259 leads to the following two equations:

$$260 \quad \sin(2c_m)/\tau = \alpha\gamma d_m/(c_m^2 + d_m^2) \quad (39)$$

261 and

$$262 \quad \sinh(2d_m)/\tau = \alpha\gamma c_m/(c_m^2 + d_m^2) \quad (40)$$

263 Noted that Eqs. (39) and (40) are respectively from the real and imaginary parts. The values of
 264 c_m and d_m can be determined by the Mathematica function FindRoot with the initial guesses
 265 of $\pi m/2$ for c_m and 10^{-4} for d_m .

266 **2.7 Pseudo-steady state solution for confined aquifers**

267 Again, when $S_y = 0$ (i.e., $\sigma = 0$), Eq. (36) reduces to $\tan \beta_m = 0$ with roots $\beta_m = 0, \pi,$
 268 $2\pi, \dots, m\pi, \dots, \infty$; factor 2 in Eq. (35) is replaced by unity. Eq. (38f) then becomes

$$269 \quad D(\bar{r}) = \begin{cases} 0 & \text{for } \beta_m \neq 0 \\ 2iK_0(\bar{r}\lambda)/(\alpha\gamma K_0(\lambda) - i\lambda K_1(\lambda)) & \text{for } \beta_m = 0 \end{cases} \quad (41)$$



270 which is obtained by applying L' Hospital's rule when $\beta_m = 0$. With Eq. (41), Eqs. (38c) and
 271 (38d) reduces, respectively, to

$$272 \quad a_s(\bar{r}) = \text{Re} \left(\frac{i K_0(\bar{r}\lambda)}{\alpha \gamma K_0(\lambda) - i \lambda K_1(\lambda)} \right) \quad (42a)$$

273 and

$$274 \quad b_s(\bar{r}) = \text{Im} \left(\frac{i K_0(\bar{r}\lambda)}{\alpha \gamma K_0(\lambda) - i \lambda K_1(\lambda)} \right) \quad (42b)$$

275 which are independent of dimensionless elevation \bar{z} , indicating horizontal confined flow.
 276 Based on Eqs. (41), (42a) and (42b), the pseudo-steady state solution for confined aquifers can
 277 be expressed as:

$$278 \quad \bar{h}_s(\bar{r}, \bar{t}) = \bar{A}_s(\bar{r}) \cos(\gamma t - \phi_s(\bar{r})) \quad (43a)$$

279 with

$$280 \quad \bar{A}_s(\bar{r}) = \sqrt{a_s(\bar{r})^2 + b_s(\bar{r})^2} \quad (43b)$$

$$281 \quad \phi_s(\bar{r}) = \cos^{-1}(b_s(\bar{r})/A_s(\bar{r})) \quad (43c)$$

282 2.8 Sensitivity analysis

283 Sensitivity analysis evaluates hydraulic head variation in response to the change in each of K_r ,
 284 K_z , S_s , S_y , and ω . The normalized sensitivity coefficient can be defined as (McCuen, 1985)

$$285 \quad S_i = P_i \frac{\partial X}{\partial P_i} \quad (44)$$

286 where S_i is the sensitivity coefficient of i th parameter; P_i is the magnitude of the i th input
 287 parameter; X represents the present solution in dimensional form. Eq. (44) can be approximated
 288 as

$$289 \quad S_i = P_i \frac{X(P_i + \Delta P_i) - X(P_i)}{\Delta P_i} \quad (45)$$

290 where ΔP_i , a small increment, is chosen as $10^{-3} P_i$.

291 3. Results and Discussion

292 In the following sections, we demonstrate the response of the hydraulic head to oscillatory
 293 pumping using the present solution. The default values in calculation are $b = 20$ m, $Q = 1$ L/s,
 294 $r_c = 0.06$ m, $r_w = 0.05$ m, $K_r = 10^{-4}$ m/s, $K_z = 10^{-5}$ m/s, $S_s = 10^{-5}$ m⁻¹, $S_y = 0.1$, $\omega = 2\pi/30$ s⁻¹, r



295 $= r_w$ and $z = 10$ m. The corresponding dimensionless parameters are $\alpha = 3600$, $\gamma = 5.24 \times 10^{-5}$,
 296 $\kappa = 0.1$, $\mu = 6.2 \times 10^{-7}$, and $\sigma = 500$. The practical ranges for dimensionless parameters are
 297 $0.1 \leq \kappa \leq 0.5$, $10 \leq \sigma \leq 10^5$, $10^{-1} \leq \alpha \leq 10^5$ and $10^{-6} \leq \gamma \leq 1$.

298 3.1. Transient head fluctuation affected by the initial condition

299 Figure 2 demonstrates dimensional hydraulic head predicted by the present transient solution
 300 $h = h_{\text{exp}} + h_{\text{SHM}}$ and the pseudo-steady state solution h_s for unconfined aquifers. The head
 301 fluctuation defined by h starts from $h = 0$ at $t = 0$ and approaches SHM that can be
 302 predicted by h_{SHM} when $h_{\text{exp}} \cong 0$ m after $t = 219$ sec. On the other hand, h_{SHM} with about
 303 13 sec shift of time predicts very close SHM to the pseudo-steady state solution with error less
 304 than 3%. This example indicates that the present transient solution h can be expressed as $h =$
 305 $h_{\text{exp}} + h_s$ with a certain time shift so that head fluctuation starts from $h = 0$ at $t = 0$.

306 Define an ignorable dimensionless head change as $|\bar{h}| < 10^{-2}$ (i.e., $|h| < 1$ mm)
 307 according to $\bar{h} = (2\pi b K_r / Q)h$ for the practical ranges of $b K_r \geq 10^3$ m²/d and $Q \leq 10^2$
 308 m³/d (Rasmussen et al. 2003). Define \bar{t}_s as a dimensionless transient time to have
 309 $\bar{h}_{\text{exp}}(\bar{r}, \bar{z}, \bar{t}) = 10^{-2}$ (or $\bar{h} \cong \bar{h}_{\text{SHM}}$). The time can be estimated using the Mathematica
 310 function FindRoot to solve the equation that

$$311 |\bar{h}_{\text{exp}}(1, 0.5, \bar{t}_s)| = 10^{-2} \quad (46)$$

312 Figure 3 displays the curve of dimensionless frequency γ versus the largest predicted \bar{t}_s . The
 313 curve is plotted based on the values of $\kappa = 0.1$, $\alpha = 10^5$ and $\sigma = 500$. When $\gamma \leq 2.7 \times 10^{-3}$,
 314 the value of \bar{t}_s decreases with increasing γ . When $\gamma > 2.7 \times 10^{-3}$, \bar{t}_s can be regarded as
 315 zero because a numerical result from the LHS function of Eq. (46) is smaller than 10^{-2} for any
 316 value of \bar{t}_s . Note that \bar{t}_s increases with decreasing κ so we choose the smallest of the
 317 practical range $0.1 \leq \kappa \leq 0.5$. Variations in dimensionless parameters σ and α have
 318 insignificant effect on \bar{t}_s prediction. The largest \bar{t}_s is about 2.45×10^6 that equals 10 min
 319 obtained by $t_s = S_s r_w^2 \bar{t}_s / K_r$, $r_w = 0.05$ m, $K_r = 10^{-4}$ m/s and $S_s = 10^{-5}$ m⁻¹. The relation between
 320 \bar{t}_s and γ can therefore be approximated as



$$\log_{10} \bar{t}_s = \begin{cases} -\sum_{k=0}^6 c_k (\log_{10} \gamma)^k & \text{for } 10^{-6} \leq \gamma \leq 2.7 \times 10^{-3} \\ 1 & \text{for } \gamma > 2.7 \times 10^{-3} \end{cases} \quad (47)$$

where $c_0 = 629.90517$, $c_1 = 874.82145$, $c_2 = 500.07155$, $c_3 = 151.54284$, $c_4 = 25.63248$, $c_5 = 2.29276$, and $c_6 = 0.08471$ obtained by the Mathematica function Fit based on least-square curve fitting. Existing models assuming hydraulic head response as SHM are applicable when $\bar{t} \geq \bar{t}_s$ provided in Fig. 3 for a known value of γ .

3.2. Radius of influence from pumping well

Researchers have paid attention to the identification of aquifer hydraulic parameters within the dimensionless radius of influence \bar{R} from an oscillatory pumping well (e.g., Cadiff and Saylor, 2016). This section quantifies \bar{R} that is dominated by the magnitude of γ . Define \bar{R} from the pumping well to a location where \bar{R} satisfies

$$\bar{A}_t(\bar{R}, \bar{z}) = 10^{-2} \quad (48)$$

where \bar{A}_t is defined in Eq. (24d), \bar{z} can be an arbitrary value of $0 \leq \bar{z} \leq 1$ because $\bar{A}_t(\bar{R}, \bar{z})$ is independent of \bar{z} , and the value 10^{-2} causes an insignificant dimensional amplitude that is defined as $Q\bar{A}_s(\bar{R}, \bar{z})/(2\pi bK_r)$ less than 1 mm for the practical ranges of $bK_r \geq 10^3$ m²/d and $Q \leq 10^2$ m³/d (Rasmussen et al. 2003). The Mathematica function FindRoot is applied to solve Eq. (48) to determine the value of \bar{R} . Figure 4 shows the attenuation of the amplitude $\bar{A}_t(\bar{r}, \bar{z})$ at $\bar{z} = 0.5$ for various values of γ in panel (a) and the curve of γ versus \bar{R} calculated by Eq. (48) in panel (b). The greater value of γ causes smaller \bar{A}_t and \bar{R} , indicating that higher frequency of oscillatory pumping, larger aquifer storage or lower aquifer horizontal conductivity leads to smaller amplitude of groundwater fluctuation and smaller radius of influence. When $\gamma > 2.8 \times 10^{-2}$, the largest dimensionless amplitude at the rim of the pumping well is less than 10^{-2} (i.e., $\bar{A}_t(1, \bar{z}) < 10^{-2}$). The magnitude of \bar{R} can therefore be considered as unity. The changes in κ and σ cause insignificant effect on the estimates of \bar{A}_t and \bar{R} . The magnitude of α related to wellbore storage effect will be discussed in the next section. With the Mathematica function Fit, the relation between \bar{R} and γ can be approximated as



$$\log_{10} \bar{R} = \begin{cases} \sum_{k=0}^6 c_k (\log_{10} \gamma)^k & \text{for } 10^{-6} \leq \gamma \leq 2.8 \times 10^{-2} \\ 0 & \text{for } \gamma > 2.8 \times 10^{-2} \end{cases} \quad (49)$$

where $c_0 = -4.13203$, $c_1 = -2.83369$, $c_2 = 0.56905$, $c_3 = 0.65943$, $c_4 = 0.18209$, $c_5 = 0.02147$
 and $c_6 = 9.33152 \times 10^{-4}$. It serves as a handy tool of estimating \bar{R} within which observation
 wells can receive signal from an oscillatory pumping well.

3.3. Effect of wellbore storage on head fluctuation

The effect of wellbore storage is dominated by the magnitude of α accounting for variation in
 the well radius. This section discusses the discrepancy due to assuming an infinitesimal radius.
 Figure 5 demonstrates the hydraulic head predicted by the present pseudo-steady state solution,
 Eq. (26), for $\alpha = 10^{-2}$, 10^{-1} , 1, 10, 10^2 and 10^3 at (a) $\bar{r} = 1$ at the rim of the pumping well and
 (b) $\bar{r} = 16$ away from the well. The Dagan and Rabinovich (2014) solution assuming an
 infinitesimal radius is taken for comparison. For the case of $\bar{r} = 1$, Fig. 5(a) indicates that the
 predicted dimensionless amplitude increases with decreasing α and remains constant when α
 $\leq 10^{-1}$. The Dagan and Rabinovich (2014) solution gives an overestimate of dimensionless
 amplitude because of neglecting the wellbore storage effect. This result differs from the finding
 of Papadopoulos and Cooper (1967) that the effect is ignorable for a large time of a constant-
 rate pumping test (i.e., $t > 2.5 \times 10^2 r_c^2 / (K_r b)$). For the case of $\bar{r} = 16$ (or $\bar{r} \geq 16$), both
 solutions agree well when $\alpha \leq 10$, indicating that the wellbore storage effect gradually
 diminishes with distance from the pumping well. The effect should therefore be considered in
 OPT models especially when observed hydraulic head data are taken close to the pumping well.

3.4. Sensitivity analysis

The normalized sensitivity coefficient S_i defined as Eq. (44) with $X = h_{\text{exp}}(r, z, t)$ in Eq.
 (24b) is displayed in Fig. 6 for the response of exponential decay to the change in each of
 parameters K_r , K_z , S_s , S_y and ω with $\omega =$ (a) $2\pi/60 \text{ s}^{-1}$ and (b) $2\pi/30 \text{ s}^{-1}$. The figure indicates that
 exponential decay is very sensitive to variation in each of K_r , K_z , S_s and ω because of $|S_i| > 0$.
 Precisely, a positive perturbation in K_r , S_s , and ω produces an increase in the magnitude of
 $h_{\text{exp}}(r, z, t)$ while that in K_z causes a decrease. It is worth noting that the coefficient S_i for S_y



is very close to zero over the entire period of time, indicating that $h_{\text{exp}}(r, z, t)$ is insensitive to the change in S_y and the subtle change of gravity drainage has no influence on the exponential decay. In addition, the sensitivity curves of K_z and S_s are symmetrical to the horizontal axis, implying that these two parameters are highly correlated (Yeh and Chen, 2007). On the other hand, the spatial distributions of the normalized sensitivity coefficient S_i defined in Eq. (44) with $X = A_t(r, z)$ in Eq. (24d) are shown in Fig. 7 for SHM amplitude in response to the changes in parameters K_r , K_z , S_s , S_y and ω for $\omega = (a) 2\pi/60 \text{ s}^{-1}$ and (b) $2\pi/30 \text{ s}^{-1}$. The figure also indicates that $A_t(r, z)$ is sensitive to the change in each of K_r , K_z , S_s and ω but insensitive to the change in S_y . From those discussed above, we can conclude that the changes in the four key parameters K_r , K_z , S_s and ω significantly affect OPT model prediction, but the change in S_y doesn't.

3.5. Application of the present solution to field experiment

Rabinovich et al. (2015) conducted a field OPT in an unconfined aquifer at the BHRS. The aquifer contains a mix of sand, gravel and cobble sediments with 20 m averaged thickness. The aquifer bottom is a clay confining unit. The pumping well fully penetrating the aquifer has 10 cm inner diameter and 11.43 cm outer diameter of PVC casing. The pumping rate can be approximated as $Q \sin(\omega t)$ with $Q = 5.8 \times 10^{-5} \text{ m}^3/\text{s}$ and $\omega = 2\pi/24 \text{ s}^{-1}$. The observation data of SHM representing time-varying hydraulic head at the pumping well after a certain period of time are plotted in Fig. 8.

The aquifer hydraulic parameters K_r , K_z , S_s , and S_y can be determined by the pseudo-steady state solutions, Eqs. (38a) and (43a), coupled with the Levenberg–Marquardt algorithm provided in the Mathematica function FindFit (Wolfram, 1991). Define the residual sum of square (RSS) as $\text{RSS} = \sum_{i=1}^m e_i^2$ and the mean error (ME) as $\text{ME} = \frac{1}{m} \sum_{i=1}^m e_i$ where e_i is the difference between predicted and observed hydraulic heads and m is the number of observation data (Yeh, 1987). The estimated parameters are $K_r = 1.034 \times 10^{-5} \text{ m/s}$, $K_z = 1.016 \times 10^{-5} \text{ m/s}$, $S_s = 8.706 \times 10^{-5} \text{ m}^{-1}$, $S_y = 5.708 \times 10^{-3}$ with $\text{RSS} = 1.184 \times 10^{-3} \text{ m}^2$ and $\text{ME} = 0.5718 \text{ m}$ for the case



399 of unconfined aquifers and $K_r = 5.035 \times 10^{-4}$ m/s, $S_s = 1.40998 \times 10^{-5}$ 1/m with $RSS = 7.454 \times 10^{-4}$ m² and $ME = 0.46683$ m for the case of confined aquifers. The estimated S_y is less than two
400 orders of the typical range of 0.01~0.3 (Freeze and Cherry, 1979), which accords with the
401 findings of Rasmussen et al. (2003) and Rabinovich et al. (2015). One reason for an
402 underestimated S_y may be because flow behaviors associated with OPT and constant-rate
403 pumping test are different especially for a high frequency (i.e., ω). The moisture exchange was
404 limited by capillary fringe between the zones below and upper the water table. Several
405 laboratory researches have focused on this subject for a short period or high frequency of an
406 oscillatory pumping test (e.g., Cartwright et al., 2003; 2005) and they confirmed that the values
407 of S_y decreases more than two orders at small period of oscillation, compared with conventional
408 instantaneous drainage.

410 Rabinovich et al. (2015) reported $K_r = 6.3833 \times 10^{-4}$ m/s, $S_s = 9.22 \times 10^{-6}$ 1/m, $S_y =$
411 8.691×10^{-4} with $RSS = 2.638 \times 10^{-3}$ m² and $ME = 0.5955$ m for the case of unconfined aquifers
412 and $K_r = 7.149 \times 10^{-4}$ m/s, $S_s = 1.214 \times 10^{-5}$ 1/m with $RSS = 3.992 \times 10^{-3}$ m² and $ME = 0.5958$ m
413 for the case of confined aquifers on the basis of the Dagan and Rabinovich (2014) solution.
414 Our work provides smaller RSSs than theirs. This may be attributed to the fact that the present
415 solution considers the effect of wellbore storage on the parameter determination. Figure 8
416 displays agreement between the observation data and the head fluctuations predicted by the
417 pseudo-steady state solution, Eq. (38a), for unconfined aquifers and Eq. (43a) for confined
418 aquifers based on those estimated parameters. This indicates that the present solution is
419 applicable to real-world OPT.

420 **4. Concluding remarks**

421 A variety of analytical solutions have been proposed so far, but little attention is paid to the
422 combined effects of wellbore storage and initial condition before OPT. This study develops a
423 new model for describing hydraulic head fluctuation due to OPT in unconfined aquifers. Static
424 hydraulic head prior to OPT is regarded as an initial condition. An equation accounting for



wellbore storage effect is specified at the rim of a finite-radius pumping well. A linearized free surface equation is considered as the top boundary condition. The analytical solution of the model is derived by the Laplace transform and finite integral transform. The sensitivity analysis of the head response to the change in each of hydraulic parameters is performed. The present solution can estimate aquifer hydraulic parameters when coupling the Levenberg–Marquardt algorithm and observation data. Our findings are summarized below:

1. The transient solution of dimensionless hydraulic head is expressed as the sum of the exponential and harmonic functions of time (i.e., $\bar{h} = \bar{h}_{\text{exp}} + \bar{h}_{\text{SHM}}$) in Eq. (24a) or (25a). The latter function can be replaced by the pseudo-steady state solution with error less than 3%.
2. The exponential function \bar{h}_{exp} defined in Eq. (24b) or (25b) accounts for the effect of the initial condition of static groundwater prior to OPT. The effect diminishes when $\bar{t} \geq \bar{t}_s$ that can be approximated by Eq. (47) for a fixed dimensionless frequency γ . Existing analytical solutions assuming SHM without the initial condition are applicable when the condition $\bar{t} \geq \bar{t}_s$ is met.
3. The magnitudes of α and \bar{r} dominate the influence of wellbore storage on predicted head fluctuation due to OPT. Neglecting the influence causes a significant overestimate of the amplitude of SHM at the pumping well (i.e., $\bar{r} = 1$) in spite of an extreme range $\alpha \leq 10^{-1}$ for very small well radius. In contrast, the influence gradually diminishes with distance from the pumping well and is ignorable when $\bar{r} \geq 16$ and $\alpha \leq 10$. Existing analytical solutions assuming an infinitesimal radius can predict accurate head fluctuation when these two conditions are met.
4. The dimensionless radius of influence \bar{R} can be estimated by Eq. (49) with a dimensionless frequency γ . Observation wells should be located in the area of $\bar{r} < \bar{R}$ for obtaining observable data of head fluctuations.
5. The sensitivity analysis suggests that the changes in four parameters K_r , K_z , S_s and ω



451 significantly affect OPT model prediction but that in S_y doesn't exert any effect.

452 **References**

453 Bakhos, T., Cardiff, M., Barrash, W., and Kitanidis, P. K.: Data processing for oscillatory
454 pumping tests, *J. Hydrol.*, 511, 310–319, 2014.

455 Black, J. H., and Kipp, K. L.: Determination of Hydrogeological Parameters Using Sinusoidal
456 Pressure Tests - a Theoretical Appraisal, *Water Resour. Res.*, 17(3), 686–692, 1981.

457 Cardiff, M., Bakhos, T., Kitanidis, P. K., and Barrash, W.: Aquifer heterogeneity
458 characterization with oscillatory pumping: Sensitivity analysis and imaging potential, *Water*
459 *Resour. Res.*, 49(9), 5395–5410, 2013.

460 Cardiff, M. and Barrash, W.: 3-D transient hydraulic tomography in unconfined aquifers with
461 fast drainage response, *Water Resour. Res.*, 47, W12518, 2011.

462 Cardiff, M. and Barrash, W.: Analytical and semi-analytical tools for the design of oscillatory
463 pumping tests, *Ground Water*, 53(6), 896–907, 2014.

464 Cardiff, M. and Sayler, C.: Strategies for avoiding errors and ambiguities in the analysis of
465 oscillatory pumping tests, *J. Hydrol.*, 540, 1016–1021, 2016.

466 Cartwright, N., Nielsen, P., and Dunn, S.: Water table waves in an unconfined aquifer:
467 Experiments and modeling, *Water Resour. Res.*, 39(12), 1330, 2003.

468 Cartwright, N., Nielsen, P., and Perrochet, P.: Influence of capillarity on a simple harmonic
469 oscillating water table: Sand column experiments and modeling, *Water Resour. Res.*, 41(8),
470 W08416, 2005.

471 Christensen, N. K., Ferre, T. P. A., Fiandaca, G., and Christensen, S.: Voxel inversion of
472 airborne electromagnetic data for improved groundwater model construction and prediction
473 accuracy, *Hydrol. Earth Syst. Sci.*, 21, 1321–1337, 2017.

474 Dagan, G. and Rabinovich, A.: Oscillatory pumping wells in phreatic, compressible, and
475 homogeneous aquifers, *Water Resour. Res.*, 50(8), 7058–7066, 2014.

476 Fokker, P. A., Salina Borello, E., Serazio, C., and Verga, F.: Estimating reservoir



- 477 heterogeneities from pulse testing, *J. Petrol. Sci. Eng.*, 86–87, 15–26, 2012.
- 478 Fokker, P. A., Renner, J., and Verga, F.: Numerical modeling of periodic pumping tests in
479 wells penetrating a heterogeneous aquifer, *Am. J. Environ. Sci.*, 9(1), 1–13, 2013.
- 480 Freeze, R. A. and Cherry, J. A.: *Groundwater*, Prentice-Hall, New Jersey, 1979, 604 pp.
- 481 Kuo, C.: Determination of reservoir properties from sinusoidal and multirate flow tests in one
482 or more wells, *SPE J.*, 12(6), 499–507, 1972.
- 483 Latinopoulos, P.: Analytical solutions for periodic well recharge in rectangular aquifers with
484 3rd-kind boundary-conditions, *J. Hydrol.*, 77(1–4), 293–306, 1985.
- 485 Liang, X., Zhan, H., Zhang, Y.-K., and Liu, J.: On the coupled unsaturated-saturated flow
486 process induced by vertical, horizontal, and slant wells in unconfined aquifers, *Hydrol. Earth*
487 *Syst. Sci.*, 21, 1251–1262, 2017.
- 488 Maineult, A., Strobach, E., and Renner, J.: Self-potential signals induced by periodic pumping
489 tests, *J. Geophys. Res: Sol. Earth*, 113(B1), B01203, 2008.
- 490 McCuen, R. H.: *Statistical methods for engineers*, Prentice Hall, 1985
- 491 Muthuwatta, L., Amarasinghe, U. A., Sood, A., and Surinaidu, L.: Reviving the “Ganges Water
492 Machine”: where and how much?, *Hydrol. Earth Syst. Sci.*, 21, 2545–2557, 2017.
- 493 Neuman, S.P.: Theory of flow in unconfined aquifers considering delayed response of the water
494 table, *Water Resour. Res.*, 8(4), 1031–1045, 1972.
- 495 Papadopoulos, I. S. and Cooper, H. H.: Drawdown in a well of large diameter, *Water Resour.*
496 *Res.*, 3(1), 241–244, 1967.
- 497 Rabinovich, A., Barrash, W., Cardiff, M., Hochstetler, D., Bakhos, T., Dagan, G., and Kitanidis,
498 P. K.: Frequency dependent hydraulic properties estimated from oscillatory pumping tests
499 in an unconfined aquifer, *J. Hydrol.*, 531, 2–16, 2015.
- 500 Rasmussen, T. C., Haborak, K. G., and Young, M. H.: Estimating aquifer hydraulic properties
501 using sinusoidal pumping at the Savannah River site, South Carolina, USA, *Hydrogeol. J.*,
502 11(4), 466–482, 2003.
- 503 Spane, F. A. and Mackley, R. D.: Removal of river-stage fluctuations from well response using



- 504 multiple regression, *Ground Water*, 49(6), 794–807, 2011.
- 505 Vine, N. L., Butler, A., McIntyre, N., and Jackson, C.: Diagnosing hydrological limitations of
- 506 a land surface model: application of JULES to a deep-groundwater chalk basin, *Hydrol.*
- 507 *Earth Syst. Sci.*, 20, 143–159, 2016.
- 508 Watlet, A., Kaufmann, O., Triantafyllou, A., Poulain, A., Chambers, J. E., Meldrum, P. I.,
- 509 Wilkinson, P. B., Hallet, V., Quinif, Y., Ruymbeke, M. V., and Camp, M. V.: Imaging
- 510 groundwater infiltration dynamics in the karst vadose zone with long-term ERT monitoring,
- 511 *Hydrol. Earth Syst. Sci.*, 22, 1563–1592, 2018.
- 512 Wolfram, S.: *Mathematica*, Version 2.0. Wolfram Research, Inc., Champaign, IL, 1991.
- 513 Yeh, H. D.: Theis' solution by nonlinear least-squares and finite-difference Newton's Method,
- 514 *Ground Water*, 25(6), 710–715, 1987.
- 515 Yeh, H. D. and Chen, Y. J.: Determination of skin and aquifer parameters for a slug test with
- 516 wellbore-skin effect, *J. Hydrol.*, 342(3–4), 283–294, 2007.
- 517 Yeh, T. C. J. and Liu, S. Y.: Hydraulic tomography: Development of a new aquifer test method,
- 518 *Water Resour. Res.*, 36(8), 2095–2105, 2000.
- 519 Zhou, Y. Q., Lim, D., Cupola, F., and Cardiff, M.: Aquifer imaging with pressure waves
- 520 evaluation of low-impact characterization through sandbox experiments, *Water Resour. Res.*,
- 521 52(3), 2141–2156, 2016.

522 Acknowledgments

523 Research leading to this paper has been partially supported by the grants from the Fundamental

524 Research Funds for the Central Universities (2018B00114), the National Natural Science

525 Foundation of China (41561134016 and 51421006) and the Taiwan Ministry of Science and

526 Technology under the contract numbers MOST 105-2221-E-009 -043-MY2 and MOST 106-

527 2221-E-009 -066. The authors would like to thank Prof. John L. Wilson for his suggestion of

528 including the wellbore effect in the OPT model.



529 **Appendix A: Finite integral transform**

530 Applying the finite integral transform to the model of Eqs. (14) – (18) results in (Latinopoulos,
 531 1985)

$$532 \quad \tilde{h}(\beta_n) = \Im\{\hat{h}(\bar{z})\} = \int_0^1 \hat{h}(\bar{z}) F_t \cos(\beta_n \bar{z}) d\bar{z} \quad (\text{A.1})$$

$$533 \quad F_t = \left(\frac{2(\beta_n^2 + a^2 p^2)}{\beta_n^2 + a^2 p^2 + ap} \right)^{0.5} \quad (\text{A.2})$$

534 where β_n is the root of Eq. (19). On the basis of integration by parts, one can write

$$535 \quad \Im\left\{\frac{\partial^2 \tilde{h}}{\partial \bar{z}^2}\right\} = \int_0^1 \left(\frac{\partial^2 \tilde{h}}{\partial \bar{z}^2}\right) F(\beta_n) \cos(\beta_n \bar{z}) d\bar{z} = -\beta_n^2 \tilde{h} \quad (\text{A.3})$$

536 Note that Eq. (A.3) is applicable only for the no-flow condition specified at $\bar{z} = 0$ (i.e., Eq.
 537 (17)) and third-type condition specified at $\bar{z} = 1$ (i.e., Eq. (16)). The formula for the inverse
 538 finite integral transform is defined as

$$539 \quad \hat{h}(\bar{z}) = \Im^{-1}\{\tilde{h}(\beta_n)\} = \sum_{n=1}^{\infty} \tilde{h}(\beta_n) F(\beta_n) \cos(\beta_n \bar{z}) \quad (\text{A.4})$$

540 Similarly, apply the transform to the model of Eqs. (27) – (31); one can have

$$541 \quad \tilde{H}(\beta_m) = \Im\{\bar{H}(\bar{z})\} = \int_0^1 \bar{H}(\bar{z}) F_s \cos(\beta_m \bar{z}) d\bar{z} \quad (\text{A.5})$$

542 where F_s is defined in Eq. (35); β_m is the root of Eq. (36). It also has the property that

$$543 \quad \Im\left\{\frac{\partial^2 \tilde{H}}{\partial \bar{z}^2}\right\} = \int_0^1 \left(\frac{\partial^2 \tilde{H}}{\partial \bar{z}^2}\right) F_s \cos(\beta_m \bar{z}) d\bar{z} = -\beta_m^2 \tilde{H} \quad (\text{A.6})$$

544 Again, Eq. (A.6) is applicable only for the no-flow condition specified at $\bar{z} = 0$ (i.e., Eq. (30))
 545 and third-type condition specified at $\bar{z} = 1$ (i.e., Eq. (29)). The inverse finite integral
 546 transform can be written as

$$547 \quad \bar{H}(\bar{z}) = \Im^{-1}\{\tilde{H}(\beta_m)\} = \sum_{m=1}^{\infty} \tilde{H}(\beta_m) F_s \cos(\beta_m \bar{z}) \quad (\text{A.7})$$



548 **Appendix B: Derivation of Eqs. (24a) – (24k)**

549 On the basis of Eq. (A.4) and taking the inverse finite integral transform to Eq. (22), one can
 550 have the Laplace-domain solution as

$$551 \quad \hat{h}(\bar{r}, \bar{z}, p) = 2 \sum_{n=1}^{\infty} \tilde{h}(\bar{r}, \beta_n, p) \cos(\beta_n \bar{z}) \quad (\text{B.1})$$

552 with

$$553 \quad \tilde{h}(\bar{r}, \beta_n, p) = \hat{h}_1(p) \cdot \hat{h}_2(p) \quad (\text{B.2})$$

$$554 \quad \hat{h}_1(p) = \frac{\gamma}{(p^2 + \gamma^2)} \quad (\text{B.3})$$

$$555 \quad \hat{h}_2(p) = -\varphi_1 \varphi_2 \quad (\text{B.4})$$

$$556 \quad \varphi_1 = \sin \beta_n K_0(\bar{r} \lambda) / \left(\beta_n (p \alpha K_0(\lambda) + \lambda K_1(\lambda)) \right) \quad (\text{B.5})$$

$$557 \quad \varphi_2 = (\beta_n^2 + a^2 p^2) / (\beta_n^2 + a^2 p^2 + a p) \quad (\text{B.6})$$

558 where λ is defined in Eq. (23). Using the Mathematica function InverseLaplaceTransform, the
 559 inverse Laplace transform for $\hat{h}_{p1}(p)$ in Eq. (B.3) can be obtained as

$$560 \quad \hat{h}_1(\bar{t}) = \sin(\gamma \bar{t}) \quad (\text{B.7})$$

561 The inverse Laplace transform for $\hat{h}_{p2}(\bar{r}, \beta_n, p)$ in Eq. (B.4) is defined as

$$562 \quad \hat{h}_2(\bar{t}) = \frac{1}{2\pi i} \int_{\xi - i\infty}^{\xi + i\infty} \hat{h}_2(p) e^{p\bar{t}} dp \quad (\text{B.8})$$

563 where ξ is a real number being large enough so that all singularities are on the LHS of the
 564 straight line from $(\xi, -i\infty)$ to $(\xi, i\infty)$ in the complex plane. The integrand $\hat{h}_2(p)$ is a
 565 multiple-value function with a branch point at $p = -\mu\beta_n^2$ and a branch cut from the point
 566 along the negative real axis. In order to reduce $\hat{h}_2(p)$ to a single-value function, we consider
 567 a modified Bromwich contour that contains a straight line \overline{AB} , \overline{CD} right above the branch cut
 568 and \overline{EF} right below the branch cut, a semicircle with radius R , and a circle \widehat{DE} with radius ε
 569 in Fig. A1. According to the residual theory and the Bromwich integral, Eq. (B.8) becomes

$$570 \quad \hat{h}_2(\bar{t}) + \lim_{\substack{\varepsilon \rightarrow 0 \\ R \rightarrow \infty}} \frac{1}{2\pi i} \left[\int_B^C \hat{h}_2(p) e^{p\bar{t}} dp + \int_C^D \hat{h}_2(p) e^{p\bar{t}} dp + \int_D^E \hat{h}_2(p) e^{p\bar{t}} dp + \right. \\ \left. \int_E^F \hat{h}_2(p) e^{p\bar{t}} dp + \int_F^A \hat{h}_2(p) e^{p\bar{t}} dp \right] = 0 \quad (\text{B.10})$$



where zero on the RHS is due to no pole in the complex plane. The integrations for paths \widehat{BA}
 (i.e. $\int_B^C \hat{h}_2(p) e^{p\bar{t}} dp + \int_F^A \hat{h}_2(p) e^{p\bar{t}} dp$) with $R \rightarrow \infty$ and \widehat{DE} (i.e. $\int_D^E \hat{h}_2(p) e^{p\bar{t}} dp$) with
 $\varepsilon \rightarrow 0$ equal zero. The path \overline{CD} starts from $p = -\infty$ to $p = -\mu\beta_n^2$ and \overline{EF} starts from
 $p = -\mu\beta_n^2$ to $p = -\infty$. Eq. (B.10) therefore reduces to

$$\hat{h}_2(\bar{t}) = -\frac{1}{2\pi i} \left(\int_{-\infty}^{-\mu\beta_n^2} \hat{h}_2(p^+) e^{p^+\bar{t}} dp + \int_{-\mu\beta_n^2}^{-\infty} \hat{h}_2(p^-) e^{p^-\bar{t}} dp \right) \quad (\text{B.11})$$

where p^+ and p^- are complex numbers right above and below the real axis, respectively.
 Consider $p^+ = \zeta e^{i\pi} - \mu\beta_n^2$ and $p^- = \zeta e^{-i\pi} - \mu\beta_n^2$ in the polar coordinate system with the
 origin at $(-\mu\beta_n^2, 0)$. Eq. (B.11) then becomes

$$\hat{h}_2(\bar{t}) = \frac{-1}{2\pi i} \int_0^\infty \hat{h}_2(p^+) e^{p^+\bar{t}} dp - \hat{h}_2(p^-) e^{p^-\bar{t}} d\zeta \quad (\text{B.12})$$

where p^+ and p^- lead to the same result of $p_0 = -\zeta - \mu\beta_n^2$ for a given ζ ; $\lambda = \sqrt{p + \mu\beta_n^2}$
 equals $\lambda_0 = \sqrt{\zeta}i$ for $p = p^+$ and $-\lambda_0$ for $p = p^-$. Note that $\hat{h}_2(p^+) e^{p^+\bar{t}}$ and
 $\hat{h}_2(p^-) e^{p^-\bar{t}}$ are in terms of complex numbers. The numerical result of the integrand in Eq.
 (B.12) must be a pure imaginary number that is exactly twice of the imaginary part of a complex
 number from $\hat{h}_2(p^+) e^{p^+\bar{t}}$ with $p^+ = p_0$ and $\lambda = \lambda_0$. The inverse Laplace transform for
 $\hat{h}_2(p)$ can be written as

$$\hat{h}_2(\bar{t}) = \frac{-1}{\pi} \int_0^\infty \text{Im}(\varphi_1 \varepsilon_2 e^{p_0 \bar{t}}) d\zeta \quad (\text{B.13})$$

where $p = p_0$; $\lambda = \lambda_0$; φ_1 and ε_2 are respectively defined in Eqs. (B.5) and (24i); $\text{Im}(-)$
 represents the numerical imaginary part of the integrand. According to the convolution theory,
 the inverse Laplace transform for $\tilde{h}(\bar{r}, \beta_n, p)$ is

$$\hat{h}(\bar{r}, \beta_n, \bar{t}) = \int_0^{\bar{t}} \hat{h}_2(\tau) \hat{h}_1(\bar{t} - \tau) d\tau \quad (\text{B.14})$$

where $\bar{h}_1(\bar{t} - \tau) = \sin(\gamma(\bar{t} - \tau))$ based on Eq. (B.7); $\bar{h}_2(\tau)$ is defined in Eq. (B.13) with
 $\bar{t} = \tau$. Eq. (B.14) can reduce to

$$\hat{h}(\bar{r}, \beta_n, \bar{t}) = \frac{-1}{\pi} \int_0^\infty \text{Im} \left(\frac{\varphi_1 \varepsilon_2 (\gamma e^{p_0 \bar{t}} - \gamma \cos(\gamma \bar{t}) - p_0 \sin(\gamma \bar{t}))}{p_0^2 + \gamma^2} \right) d\zeta \quad (\text{B.15})$$



595 Substituting $\tilde{h}(\bar{r}, \beta_n, p) = \hat{h}(\bar{r}, \beta_n, \bar{t})$ and $\hat{h}(\bar{r}, \bar{z}, p) = \bar{h}(\bar{r}, \bar{z}, \bar{t})$ into Eq. (B.1) and

596 rearranging the result leads to

$$597 \quad \bar{h}(\bar{r}, \bar{z}, \bar{t}) = \frac{-2}{\pi} \sum_{n=1}^{\infty} \int_0^{\infty} \cos(\beta_n \bar{z}) \operatorname{Im}(\varepsilon_1 \varepsilon_2 \gamma e^{p_0 \bar{t}}) d\zeta +$$

$$598 \quad \frac{2}{\pi} \sum_{n=1}^{\infty} \int_0^{\infty} \cos(\beta_n \bar{z}) \operatorname{Im}(\varepsilon_1 \varepsilon_2 (\gamma \cos(\gamma \bar{t}) + p_0 \sin(\gamma \bar{t}))) d\zeta \quad (\text{B.16})$$

599 where ε_1 and ε_2 are defined in Eqs. (24h) and (24i); the first RHS term equals $\bar{h}_{\text{exp}}(\bar{r}, \bar{z}, \bar{t})$

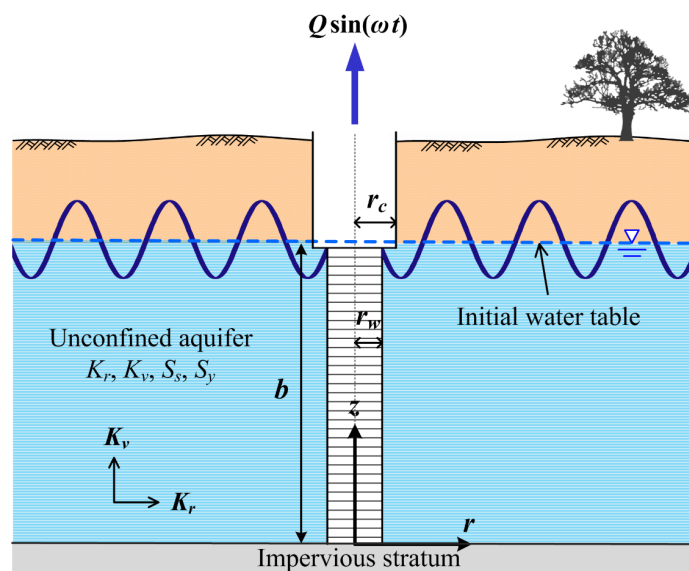
600 defined in Eq. (24b); the second term can be expressed as $\bar{h}_{\text{SHM}}(\bar{r}, \bar{z}, \bar{t})$ defined in Eq. (24c).

601 Finally, the complete solution is expressed as Eqs. (24a) – (24k).



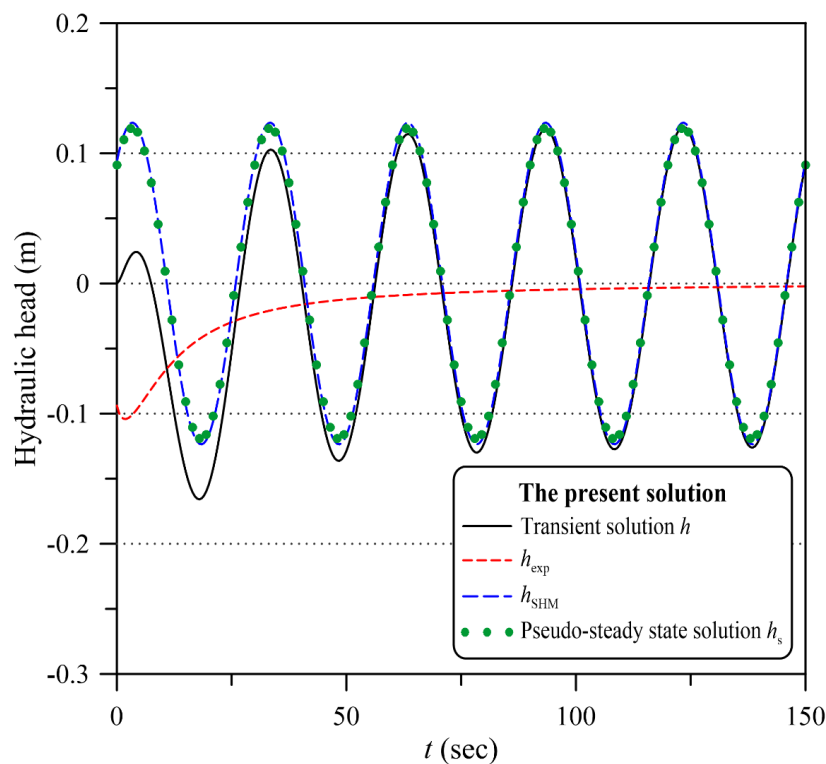
602

Figures



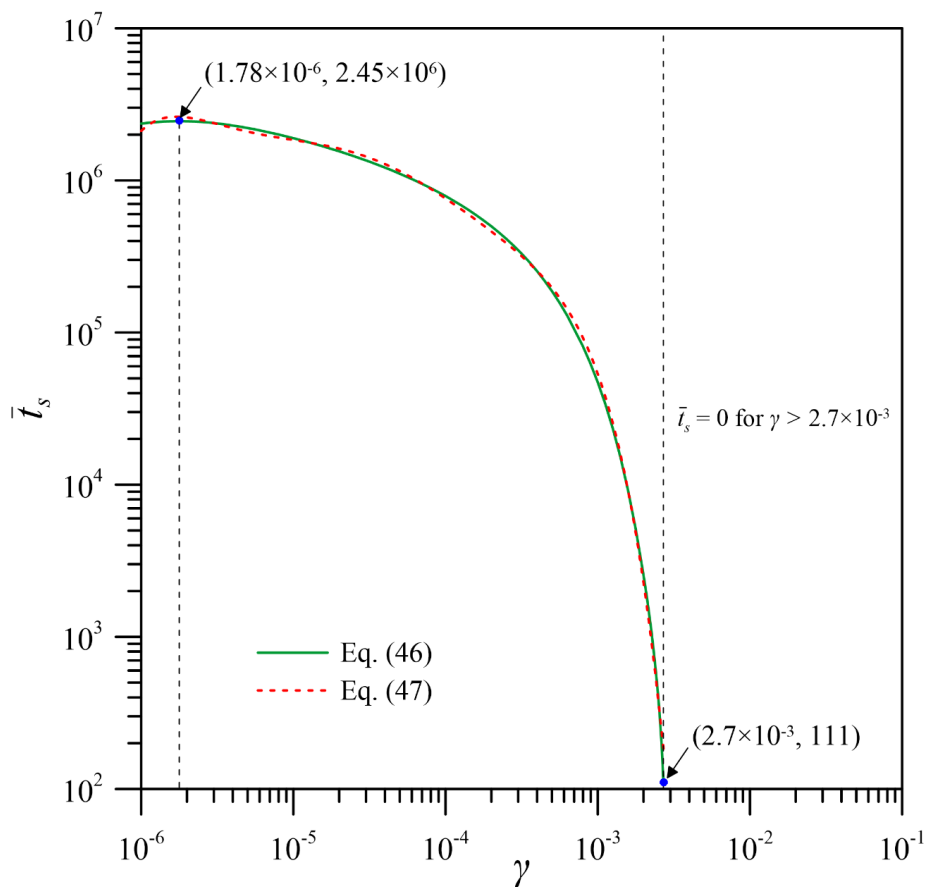
603

604 **Figure 1.** Schematic diagram for an oscillatory pumping test at a fully penetrating well of
 605 finite radius in an unconfined aquifer



606

607 **Figure 2.** Hydraulic head predicted by the transient solution expressed as $h = h_{\text{exp}} + h_{\text{SHM}}$
 608 and the pseudo-steady state solution h_s for unconfined aquifers



609

610 **Figure 3.** The curve of dimensionless frequency γ of oscillatory pumping rate versus the
 611 dimensionless time at which hydraulic head fluctuation can be regarded as SHM

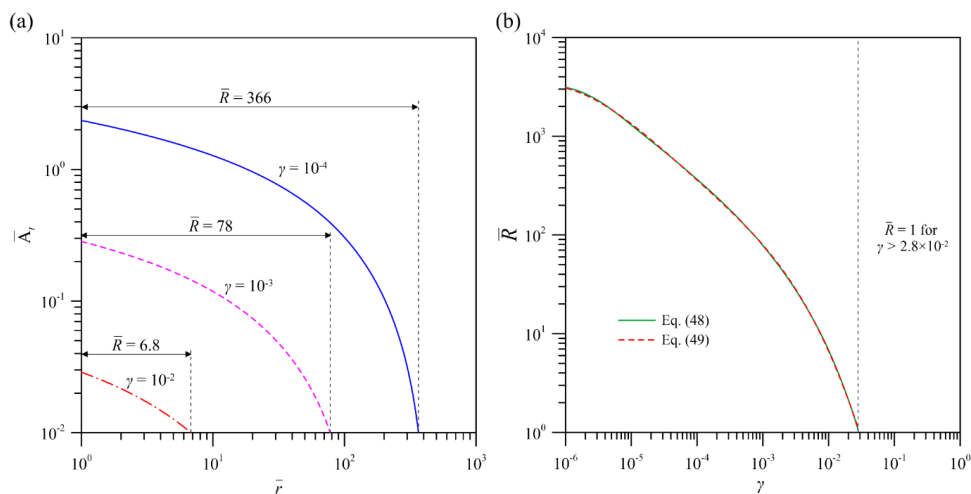
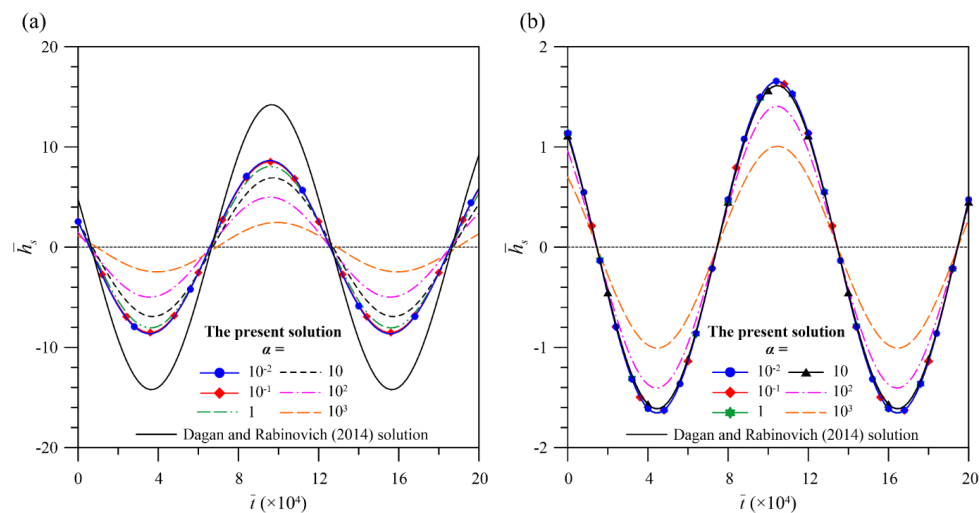
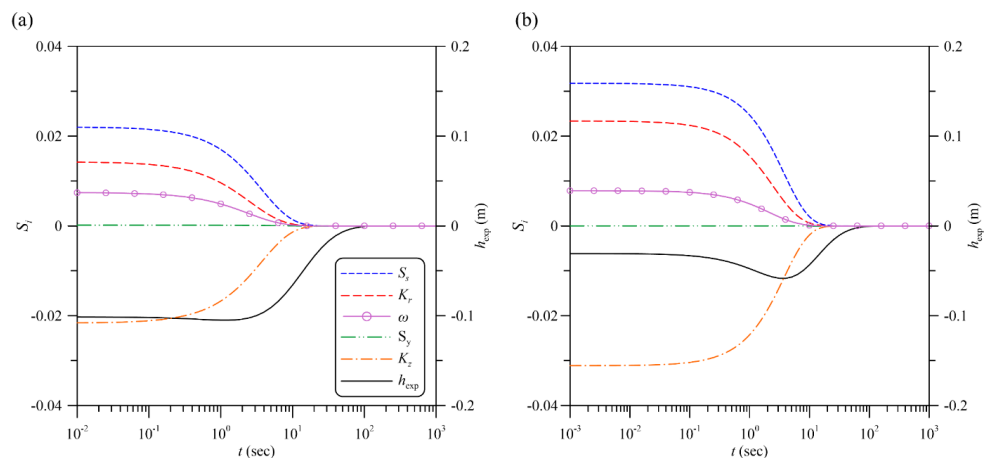


Figure 4. (a) Attenuation of dimensionless amplitude and (b) dimensionless radius of influence for different dimensionless frequency γ of oscillatory pumping rate for unconfined aquifers



616

617 **Figure 5.** Predicted Head fluctuations for (a) $\bar{r} = 1$ at the rim of the pumping well and (b) \bar{r} 618 $= 16$ away from the well using the Dagan and Rabinovich (2014) solution and the present619 solution with different α related to wellbore storage effect for unconfined aquifers



620

621 **Figure 6.** Temporal distributions of the normalized sensitivity coefficient S_i associated with
622 the exponential component defined in Eq. (24b) for parameters K_r , K_z , S_s , S_y and ω when $\omega =$
623 (a) $2\pi/60 \text{ s}^{-1}$ and (b) $2\pi/30 \text{ s}^{-1}$

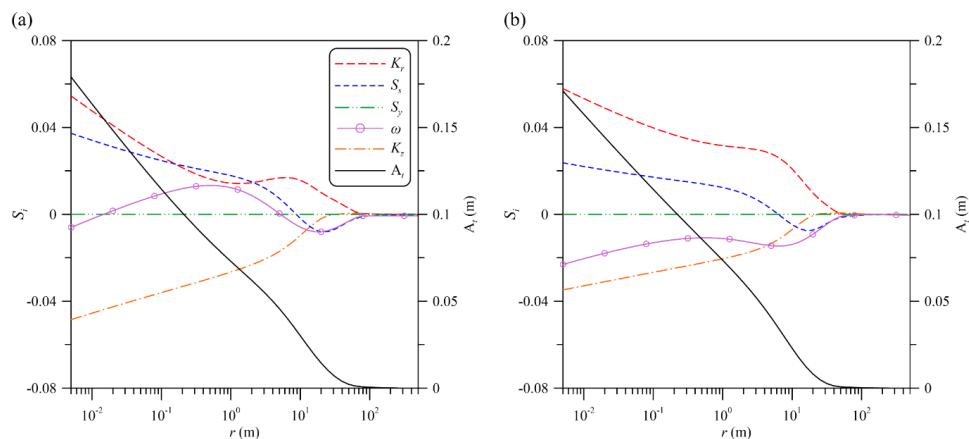
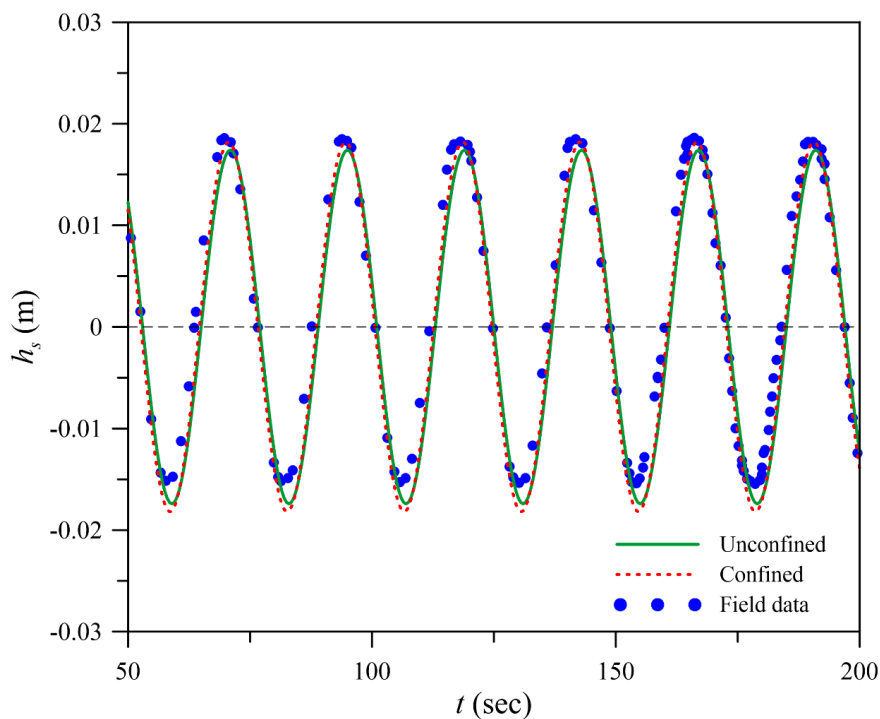
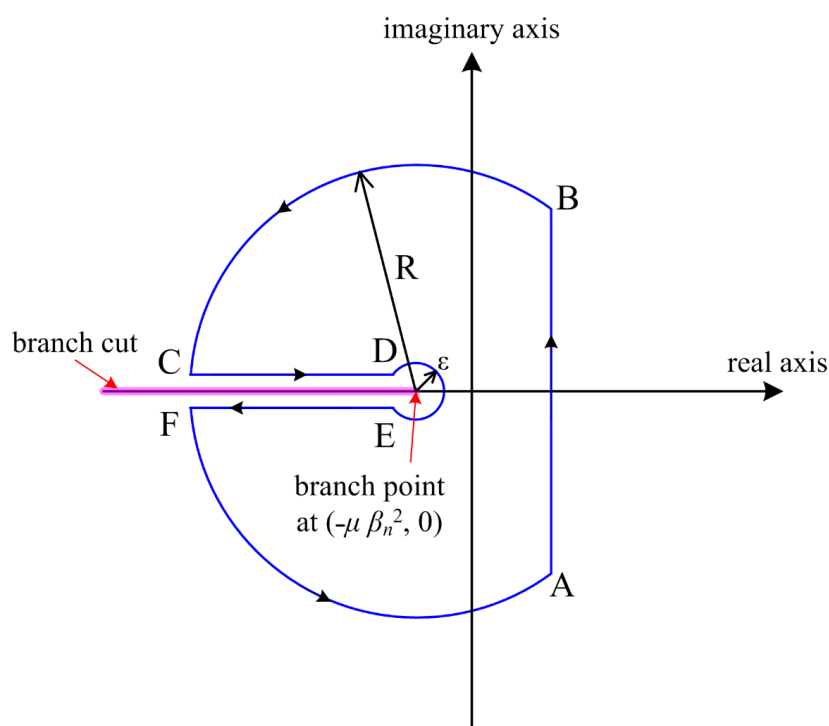


Figure 7. Spatial distributions of the normalized sensitivity coefficient S_i associated with SHM amplitude defined in Eq. (24d) for each of parameters K_r , K_z , S_s , S_y , and ω when $\omega =$ (a) $2\pi/60 \text{ s}^{-1}$ and (b) $2\pi/30 \text{ s}^{-1}$



628

629 **Figure 8.** Comparison of field observation data with head fluctuations predicted by the
630 pseudo-steady state solutions Eq. (38a) for unconfined aquifers and Eq. (43a) for confined
631 aquifers



632

633 **Figure A1.** Modified Bromwich contour for the inverse Laplace transform to a multiple-value
 634 function with a branch point and a branch cut

